

Robust 3D Features for Matching between Distorted Range Scans Captured by Moving Systems

Xiangqi Huang*, Bo Zheng*, Takeshi Masuda†, Katsushi Ikeuchi*

* The University of Tokyo

{huang, zheng, ki}@cvl.iis.u-tokyo.ac.jp

† AIST

t.masuda@aist.go.jp

Abstract

Laser range sensors are often demanded to mount on a moving platform for achieving the good efficiency of 3D reconstruction. However, such moving systems often suffer from the difficulty of matching the distorted range scans. In this paper, we propose novel 3D features which can be robustly extracted and matched even for the distorted 3D surface captured by a moving system. Our feature extraction employs Morse theory to construct Morse functions which capture the critical points approximately invariant to the 3D surface distortion. Then for each critical point, we extract support regions with the maximally stable region defined by extremal region or disconnectivity. Our feature description is designed as two steps: 1) we normalize the detected local regions to canonical shapes for robust matching; 2) we encode each key point with multiple vectors at different Morse function values. In experiments, we demonstrate that the proposed 3D features achieve substantially better performance for distorted surface matching than the state-of-the-art methods.

1. Introduction

With the emergence of accurate and long-range laser sensors, efficient 3D reconstruction of large-scale objects, such as heritage objects or urban environment, demands the dynamical sensing techniques that often mount a sensor on a moving platform, e.g., a vehicle [15], a drone [20], or a balloon [3] (shown in Fig. 1(a)). However, behind the physical convenience and efficiency brought by these dynamic sensing systems, range scans are often distorted due to the motion of sensors (as an example shown in Fig. 1(b)). This shortcoming may significantly inhibit its development, and therefore matching such kind of distorted data becomes an essential issue for reconstruction, recognition, rectification, etc.

In this paper, we present novel 3D features which are

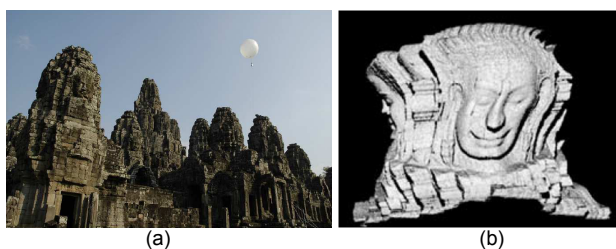


Figure 1. An example of dynamic sensing system in [3]: (a) balloon mounted with a laser range sensor. (b) a distorted range scan captured by the balloon sensor.

approximately invariant to the distortion caused by moving systems. Our method consists of two main components:

1) **Feature detection:** We first introduce Morse theory for deriving Morse functions which can robustly represent a distorted surface with critical points invariant to surface distortion. We take the critical points of local extrema as our key points and then capture the maximally stable regions on the Morse function as our support regions. Through defining the region stability by i) maximal extreme regions and; ii) maximal disconnected regions, we derive the *maximally stable extreme region* (MSER) feature (mathematically equivalent to [16]) as well as a novel feature termed *maximally stable disconnected region* (MSDR). Both methods show the good performances in our image matching results.

2) **Feature description:** Given support regions, our feature description is designed with two processes: i) canonical shape normalization; ii) description with multi-scale regions. We first normalize the detected regions to canonical shapes based on an assumption that the local region changes can be approximated as affine transformations; then we encode one key point by several support regions extracted at different scales (Morse function values).

To achieve the goal of matching distorted range images from a large number of laser scans, we make the following novel contributions in comparison with the most recent

work in dealing with deformed non-rigid objects [5, 25].

1, We apply Morse theory to define Morse functions which can robustly capture the critical points to range scans with distortion.

2, We derive the maximally stable regions for critical points (of index 0 and 2) by a novel maximal disconnectivity detection using Disconnectivity Graph (DG).

3, We propose to normalize the local support regions to canonical shapes for robust matching, and thus the regions can be simply encoded by a rotation-invariant descriptor such as Spin Image [12].

In experiments, we demonstrate that the algorithm achieves a substantially better performance for i) repeatability of feature extraction; and ii) precision of 3D surface matching in comparison with the state-of-the-art methods on both synthesized and real datasets.

2. Related work

Our work is related to three research streams in the literature of 3D features.

1. Volumetric features Despite of 2D image features (*e.g.*, SIFT, SURF, MSER [16] *etc.*) getting their success in the field, 3D shape features remain a largely unexplored topic. Extensions from 2D image features, 3D SURF [13], 3D-SIFT [8], Mean shift 3D [19], and polynomial feature [27] are designed to extract features in 3D volumetric space. These methods are very useful for medical image analyzing, shape recognition, and shape retrieval. However, for range scans, since each scan is an open surface, the volumetric features may introduce the ambiguities due to the incomplete boundaries and volumes.

2. Scale-invariant features While both DoG and SURF are grounded on the approximation of the Laplacian-of-Gaussian kernel, the MSER finds thresholded regions whose areas are maximally stable as the level changes. These ideas therefore inherently adapt to 3D geometry invariant to scale (*e.g.*, [25, 18, 17, 23, 21]), and MSER based robust local region extraction (*e.g.*, [7, 14]). The most related to our work is the Critical Nets feature proposed by Gu *et al.* [10] based on 2D image matching. Our method first extends the idea on 3D surface matching. Beyond that our method is designed as a region-based feature which takes advantage of the disconnectivity on a Morse function to detect the maximally stable region rather than a scaled region.

3. 3D features for non-rigid objects 3D feature on Non-rigid objects has a long history in medical imaging and computer vision, resulting in sophisticated techniques for matching the deformed 3D shapes [26, 22, 14, 5, 21, 25]. These techniques primarily aim to match two or more reasonably complete representatives from a deformed object class. Our work aims to match spatially distorted range images from a large number of laser scans, each of which covers only a small part of the scene and is distorted by

relative motion between range sensors and objects. Real-world scenes can have detailed geometric features at multiple scales. Our approach is thus designed to capture such features that have rarely been addressed with the techniques for non-rigid object classification.

3. Feature Detection

3.1. Morse Theory

Although the Morse theory is already studied [24] [11] in vision applications, this paper explores feature detection. Here we suppose a 3D scan is a two dimensional manifold M which can be measured by a real valued function $f: M \rightarrow \mathbb{R}$ called Morse function described as

$$f(\mathbf{x}) = r, \quad (1)$$

where for any vertex $\mathbf{x}(\in M)$ can be mapped to a real number r .

Definition 1 (Region) *If a differential manifold M can be measured by the Morse function f (smooth and real valued) in Eq.(1), for a given real number t , a region (subset) of M can be defined as:*

$$M_{\leq t} = \{\mathbf{x} \in M : f(\mathbf{x}) \leq t\}. \quad (2)$$

Note that $M_{\leq t}$ is a region with boundary, and it may be composed of a set of disjoints, multiple connected components. Following the Morse theory introduced by Goresky and Macpherson [9], recall that a point $\mathbf{x} \in M$ where the differential df of f vanishes ($\frac{df}{d\mathbf{x}} = \mathbf{0}$) is called a *critical point* of f , and the corresponding value of $f(\mathbf{x})$ is called a critical value. Morse theory considers the topological changes to the set $M_{\leq t}$ as t varies.

Theorem 1 *Let f be a differentiable function on a compact smooth manifold M . As t varies within the open interval between two adjacent critical values, the topology of $M_{\leq t}$ remains constant. [9]*

Theorem 1 tells us that the topology of $M_{\leq t}$ only changes at critical points. Furthermore, the *Morse index* λ at a critical point (defined to be the number of negative eigenvalues of the Hessian matrix) can be used to determine how the topology of $M_{\leq t}$ changes when t crosses a critical point \mathbf{x}_c . Here, the Morse index can take on a value of 0, 1 or 2 since the Hessian matrix is 2×2 for a 2-dimensional manifold.

In our case, when $\lambda = 0$, the critical point \mathbf{x}_c is a local minimum of $f(\mathbf{x})$. When $\lambda = 1$, \mathbf{x}_c is a saddle point, and the topological change is equivalent to gluing opposite sides. Finally when $\lambda = 2$, \mathbf{x}_c is a local maximum.

In this paper, we assume that the scan distortion caused by sensor motion would not make the topology change. In other words, the critical points would not change under the surface being distorted. Based on this assumption, we design our Morse functions to evaluate the surface under the deformation.

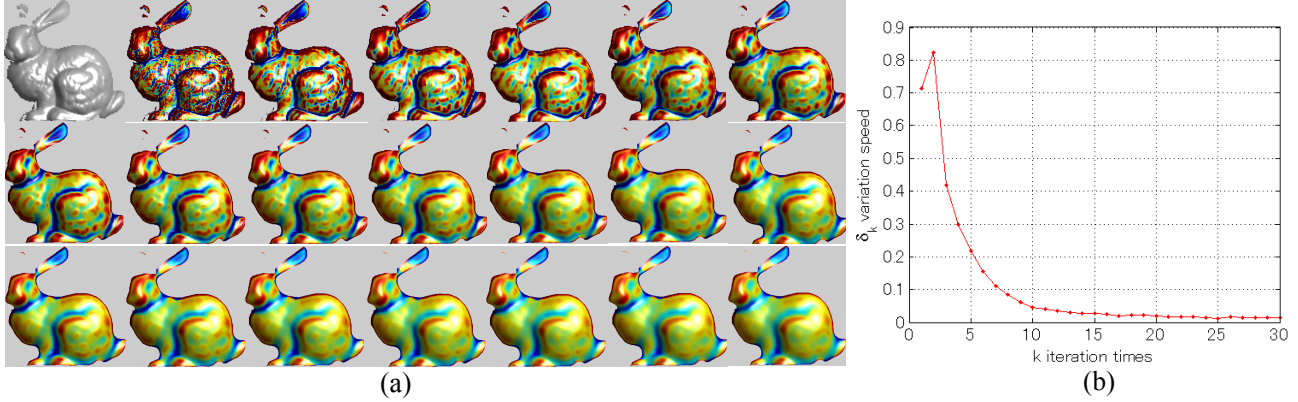


Figure 3. (a) Difference of Laplacian on bunny model. (b) Shows the speed δ_k versus the iteration times k of Laplacian.

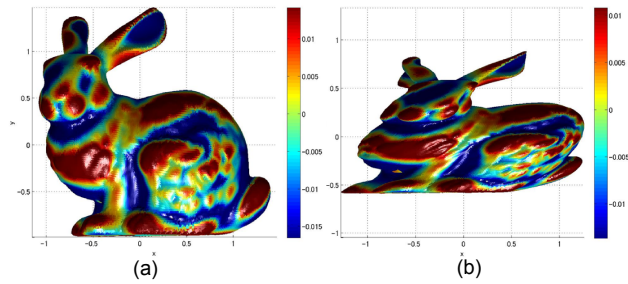


Figure 2. Bunny models colored by Morse value of IP fits: (a) the original model and (b) a distorted model.

3.2. Make it Morse

In the common case of 3D scans, the 3D surface itself cannot be guaranteed by the continuity and smoothness. So now the question is “how can we make a Morse function?” A naive method is that we can use a smooth function to fit the original shapes to make it differentiable. Actually beyond differential property, in our case, the Morse function should be able to robustly measure the critical points despite of distortion. In this paper, we explore two types of smooth functions: 1) implicit polynomial fits; and 2) β -stable Laplacian.

Implicit Polynomial An n -degree *implicit polynomial* (IP) algebraically defines a C^n function:

$$f(\mathbf{x}) = \sum_{0 \leq i, j, k; i+j+k \leq n} a_{ijk} x^i y^j z^k \quad (3)$$

where $\mathbf{x} = (x, y, z)$ is one point in the data set. An IP fit can be obtained from original dataset by a linear least-squared fitting and the degree n can be adaptively determined according to fitting accuracy proposed by Zheng *et al.* [28]. In this case, we suppose the data set would not be a simple geometry, such as a sphere, so that the Morse function (3) is not differentiable on \mathbf{x} .

Fig. 2 shows two 3D models (original and deformed), each of them is colored by the value of its Morse function,

the 8-degree IP fit. The correspondences on the two models show similar color distributions.

β -stable Laplacian Different from IP Morse function that describes the global geometry, another choice is to find a smooth function from local geometry. Our idea is inspired from the β -stable Laplacian proposed by Gu *et al.*, [10] that calculates the difference of Gaussian (DoG) operation over times on image intensities, and stops when the number of extrema on the DoG maps is stable after β -time operations. Based on this idea, we construct our Morse function using difference of Laplacian (DoL) on 3D mesh.

A single Laplacian operation on a vertex can be simply defined by a function $\mathcal{L}: \mathbb{R}^3 \rightarrow \mathbb{R}^3$

$$\mathcal{L}(\mathbf{x}_i) = \sum_{j \in \mathcal{N}(i)} \omega_{ij} (\mathbf{x}_j - \mathbf{x}_i), \quad (4)$$

where $\mathcal{N}(i)$ denotes the neighborhood of point \mathbf{x}_i , and a choice of weights is: $\omega_{ij} = \frac{\xi_{ij}}{\sum_{k \in \mathcal{N}(i)} \xi_{ik}}$ with $\xi_{ij} = 1$. Then we can define the DoL function $f_k(\mathbf{x})$ at the k -th Laplacian operation as:

$$f_k(\mathbf{x}) = \text{sign}(\mathbf{n} \cdot (\mathcal{L}_k(\mathbf{x}) - \mathcal{L}_{k-1}(\mathbf{x}))) \|\mathcal{L}_k(\mathbf{x}) - \mathcal{L}_{k-1}(\mathbf{x})\|_2 \quad (5)$$

where \mathbf{n} is the surface normal at \mathbf{x} .

Support function $N(k)$ denotes the variation at the k th-step over all points on the surface: $N(k) = \sum_i |f_k(\mathbf{x}_i)|$, then the variation speed can be defined as $\delta_k = \frac{\partial N}{\partial k}$.

Our Morse function is defined as β -stable DoL:

$$f_k(\mathbf{x}), \text{ s.t. } \delta_\epsilon < \sigma, \epsilon \in [k, k + \beta], \quad (6)$$

where σ is a threshold close to 0.

Fig. 3 (a) shows the models colored by value of DoL and changed by Laplacian operation in several times. Fig. 3 (b) shows the variation speed versus δ_k . The function tends to be 5-stable after $k \geq 15$, by setting $\sigma = 0.02$.

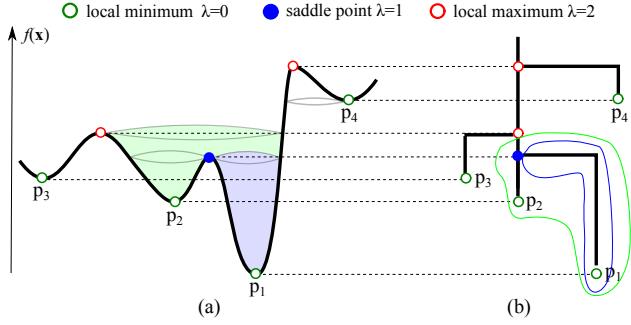


Figure 4. MSDR illustration: (a) for key point p_1 , it owns its first MSDR (in light blue) before it connects to p_2 , and it owns its second MSDR (in both green and light blue) before it connects to p_3 . (b) Disconnectivity graph (DG). p_1 's two MSDRs are corresponding Subgraphs in color respectively.

3.3. Maximally Stable Region

Here we use the term of *maximally stable region* (MSR), inspired by MSER [16]. In this paper, we derive two types of region stabilities based on the Morse functions mentioned above: 1) maximally stable extremal region (MSER); and 2) maximally stable disconnected region (MSDR). The former succeeds to original MSER theory [16], while the latter defines the maximal stability when the topology changes are detected.

According to Morse theory, the topology of a region (a smooth manifold) is very closely related to the critical points of the Morse function defined on the 3D surface. Given a region $M_{\leq t}$ defined in Eq.(2).

Maximally stable extremal region (MSER): If a connected component of $M_{\leq t}$ contains only one extreme, it defines an extremal region. For an extremal region $M_{\leq t}$ ($t \in [a, b]$), it may be possible to expand or contract by increasing t . Let $|\cdot|$ denote the cardinality (or area) of a region, then the maximal stability on the extremal region can be defined as:

$$M_{\text{MSER}} = \arg \max_t \frac{|M_{\leq t}|}{\frac{\partial}{\partial t} |M_{\leq t}|}. \quad (7)$$

Maximally stable disconnected region (MSDR): In this paper, we consider another region stability which may be detected when topological change to $M_{\leq t}$ occurs. According to Theorem 1, as t is increased, a connected component may fail to remain as a region if a second minimum is introduced to the region. This topological change to $M_{\leq t}$ only occurs at critical points. Consequently, a MSDR can be defined as:

Definition 2 (MSDR) *if a region $M_{\leq t}$ with only one connected component, then a MSDR is the maximal region that*

maintains the same number of local minima:

$$M_{\text{MSDR}} = \arg \max_t |M_{\leq t}|, \text{ s.t. } \frac{\partial |M_{\leq t}|_{\# \text{min}}}{\partial t} = 0, \quad (8)$$

where $|\cdot|_{\# \text{min}}$ denotes the number of local minima in the region.

Fig. 4 (a) shows an example that the first MSDR of p_1 is illustrated in light blue which maintains one local minimum to be maximal. With t increasing, p_1 owns its second MSDR shown as the green and light blue regions which maintain two local minima to be maximal.

To achieve this, we design our MSDR detection in Algorithm 1 by 1) we consider a 3D mesh as a graph $\mathcal{G} = (\mathcal{V}, \mathcal{E})$, where \mathcal{V} denotes the vertices and \mathcal{E} refers to the undirected edges connecting the vertices; 2) we suppose a connected component $M_{\leq t}$ in 3D mesh as a subgraph of \mathcal{G} , which might be small with only one vertex; and 3) we introduce *Disconnectivity Graph* (DG) to represent the topological structure for the manifold, which has been used in studying the potential energy in physics and chemistry [4].

Fig. 4 (b) shows a DG example that each leaf node denotes a local minimum while an inner node stands for a saddle or a local maximum, and MSDR can be viewed as a sub-tree in the DG.

4. Feature Description

Having the support regions, the next mission is to find an appropriate descriptor which can characterize the distorted regions. To this end, we assume that the local deformations on distorted surfaces can be approximately treated as affine transformations. Actually this assumption satisfies most cases since the sensors always move along the object surfaces. Therefore, we first apply a region normalization technique proposed by Cao *et al.* [6] to transform the regions to canonical shapes. We then construct a multi-scale descriptor made by a set of Spin Images.

4.1. Region Normalization

Inspired by the idea in [6] that normalizes 2D shapes into canonical shapes invariant to Affine transformations, we expand this technique to our 3D regions detected by the above process.

Denote $\mathbb{I}_{\mathcal{R}}$ as the indicator function of a region (solid shape) \mathcal{R} , assuming that \mathcal{R} is previously translated so that its barycenter is at the origin of the 3D space. The moment of order (p, q, k) (p, q and k are natural integers) of \mathcal{R} is defined by:

$$\mu_{p,q,k}(\mathcal{R}) = \int_{\mathbb{R}^3} x^p y^q z^k \mathbb{I}_{\mathcal{R}}(x, y, z) dx dy dz \quad (9)$$

Algorithm 1: MSDR Extraction

Data: $\mathcal{G} = (\mathcal{V}, \mathcal{E}); f(\mathcal{V}) \in [a, b]$
Result: a set of key points $\{P_i\}$ with corresponding MSDRs $\mathcal{R}_{P_i}^j$

```

1  % Construct disconnected graph  $\mathcal{DG}$ 
2  for  $t = a \rightarrow b$  do
3      Calculate manifold  $G_{\leq t}$ ;
4      Calculate connected components  $\{M_{\leq t}^i\} (\in G_{\leq t})$ ;
5      if new components appear then
6          Update the list of key points  $\{P_i\}$ 
7          (add the minima of new  $M_{\leq t}^i$ s into list);
8          Update  $\mathcal{DG}$ 
9          (add new key points as leaf nodes at  $t$ );
10     end
11     if new connections appear between  $\{P_i\}$  then
12         Update  $\mathcal{DG}$ 
13         (Record  $t$  as a parent node for connected  $P_i$ s);
14     end
15 end
16 % Calculate MSDRs from  $\mathcal{DG}$ 
17 for  $i = 1 \rightarrow |P|$  do
18     Revisit path  $\{t_j^i\}$  from  $P_i$  to the root of  $\mathcal{DG}$ ;
19     for  $j = 1 \rightarrow |t_j^i|$  do
20         Get MSDRs  $\mathcal{R}_{P_i}^j$  for  $P_i$ , i.e. the connected
21         component  $M_{\leq t_j^i}^i$ ;
22     end
23 end

```

Let $\mathcal{S}_{\mathcal{R}}$ be the following 3×3 positive-definite, symmetric matrix:

$$\mathcal{S}_{\mathcal{R}} = \frac{1}{\mu_{0,0,0}} \begin{bmatrix} \mu_{2,0,0} & \mu_{1,1,0} & \mu_{1,0,1} \\ \mu_{1,1,0} & \mu_{0,2,0} & \mu_{0,1,1} \\ \mu_{1,0,1} & \mu_{0,1,1} & \mu_{0,0,2} \end{bmatrix}. \quad (10)$$

Then, according to the uniqueness of Cholesky factorization, the decomposition of $\mathcal{S}_{\mathcal{R}}$: $\mathcal{S}_{\mathcal{R}} = B_{\mathcal{R}} B_{\mathcal{R}}^T$ may be unique, where $B_{\mathcal{R}}$ is a lower-triangular real matrix with positive diagonal entries. Then the normalized region associated to \mathcal{R} is the shape $\mathcal{R}' = B_{\mathcal{R}}^{-1}(\mathcal{R})$ (See [6]). It can be proved that the normalized shape \mathcal{R}' is invariant to affine transformations.

Fig. 5 illustrates the canonical shapes normalized from the models with/without distortions. We can see that the corresponding areas in the two models show similar shapes in different orientations.

4.2. Multi-scale Description

Since one key point can own one or more support regions, we need to describe multi-regions with a set of descriptors. Since our normalized support regions remain ro-

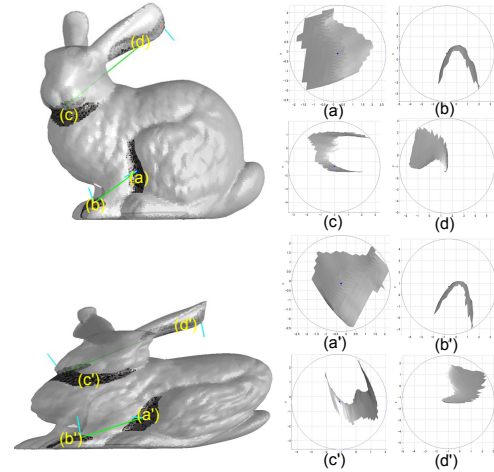


Figure 5. Canonical shapes normalization in comparison of the original model (top left) and the distorted model (bottom left) with regions (a)-(d) corresponding to (a')-(d').

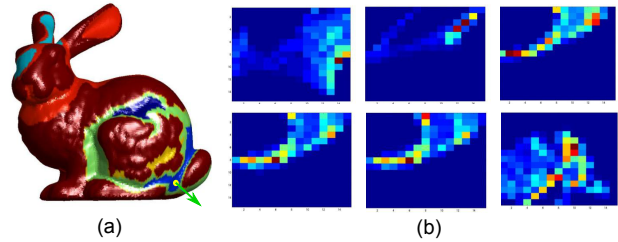


Figure 6. An example of multi-scale spin images: (a) Key point illustrated by the green arrow. (b) illustration spin images of (a) for support regions detected at different levels.

tation variation in the feature, we adopt Spin image [12] (invariant to rotation) as the basic descriptor.

To use spin image in our algorithm, for each support region R_P^j belonging to the key point P , a spin image is calculated, as shown in Fig. 6 (b). Since the size of each support region R_P^j is different, the coordinates range of α and β of the spin image is set as the maximal distance along each coordinate axis from the key point to the furthest point in the region. The resolution of bins in the accumulator is set as the same for all regions.

Given the spin image SI_j for each support region R_P^j , We construct our descriptor of the key point P as: $D(P) = \{SI_1, SI_2, \dots, SI_N\}$. Then the similarity of the two key points P and Q is defined as the minimal pairwise distance of spin images between their supporters:

$$d(P, Q) = \min_{SI_i \in \{D(P)\}, SI_j \in \{D(Q)\}} \|SI_i - SI_j\| \quad (11)$$

5. Computational Complexity

For all the procedures described above, there are mainly three steps affecting the final computational complexity:

1, Building Morse functions: while the incremental implicit polynomial modeling proposed in [28] got a similar computational cost to linear least squared method, building beta-stable Laplacian requires $O(k * |V|)$, where k is the iteration number of Laplacian operations and $|V|$ is the number of vertices.

2, MSER/MSDR generation: depth-first searching algorithm is adopted to calculate disconnected graphs, it requires $O(L * |E|)$ where L is the discretized number of value of Morse function and $|E|$ is the number of mesh edges. Although MSER has a faster implementation for 2D images in [16]), extending this technique to 3D mesh is beyond the scope of this paper.

3, Feature description: calculating a descriptor for a region requires $O(|SR|)$, where $|SR|$ stands for the number of vertices included in the region.

6. Experimental Results

We evaluate our method in terms of 1) repeatability for feature detection; 2) recall v.s. 1-precision for matching; and 3) real range data matching. All these evaluations are based on a synthesized data set and a real data set. For the synthesized data set, we collect around 30 models from the Stanford and AIM@Shape 3D scanning repository [1, 2], and selected several famous models shown in Fig. 7-10. For the real data set, we adapt our method on a large data set including 1.2-Terabyte range scans using different types of laser scanners [3], we show the selected matching results in Fig. 11 with distorted data caused by simulated motion of a balloon sensor. we compare our results with two alternatives: Heat Kernel Signature (HKS) [22] and Mesh DoG [25] which are designed for non-rigid objects matching and thus may be suitable to the distortion problem. For each method we use default parameter settings. We also compare 4 methods generated from the combinations of two Morse functions (IP and β -stable Laplacian) and two maximal stability regions (MSER [16] and MSDR) proposed in this paper.

Repeatability v.s. Deformation As shown in Fig. 7, we transform the bunny model into 13 deformed models by affine transformations to different extents. In this way, since the ground truth can be known by inverse transformations, we compare the methods mentioned above by evaluating the repeatability between the original model and transformed models. In Fig. 7, we show both the matching precision and relative repeatability defined in [17] according to the deformed models. For the other models shown in Fig. 9, we compare the repeatability for IP and Laplacian.

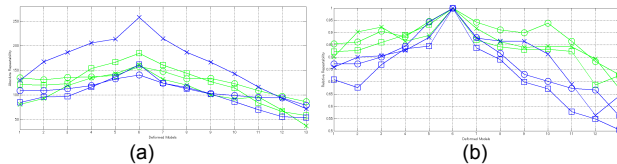


Figure 8. Absolute Repeatability (a) and Relative Repeatability (b) comparison for Morse functions on three models: IP in green and β -stable Laplacian in blue. Line markers circle, square and cross corresponding to the models shown in Fig. 9, bust, dragon and Buddha respectively.

Recall v.s. 1–Precision As the qualitative matching results shown in Fig. 9, compared with HKS and Mesh DoG [22, 25] our 4 candidates show better precision for matching. We also evaluate these 4 matching cases in Fig. 10 by the criterion Recall v.s. 1–Precision, where recall is defined as:

$$\text{recall} = \frac{\#\text{correct matches}}{\#\text{correspondences}}$$

Then the number of false matches relative to the total number of matches is represented by 1-precision:

$$1 - \text{precision} = \frac{\#\text{false matches}}{\#\text{correct matches} + \#\text{false matches}}$$

Matching results on a real data set [3] We show the distorted data matching results by the method β -stable+MSDR in Fig. 11 in both successful cases (a)-(c) and a failure case (d). The data distortion is caused by the simulated motion that a sensor mounted on a balloon captures data in air (see Fig. 1(a)).

7. Conclusion

We present a novel approach for detecting and describing 3D features based on Morse theory. Facing the problem of range scan distortion, the proposed β -stable Morse function combined with MSDR are proved to be superior to the others including the popular non-rigid methods [22, 25]. We demonstrate its feasibility in experiments and show that this provides an interesting way of dynamic sensing, because the robust matching of distorted range scans provides the good initials for non-rigid region to the data rectification.

Acknowledgment

This work is supported by Next-generation Energies for Tohoku Recovery (NET), MEXT, Japan.

References

- [1] <http://graphics.stanford.edu/data/3Dscanrep/>.
- [2] <http://shapes.aimatshape.net/>.
- [3] A. Banno, T. Masuda, T. Oishi, and K. Ikeuchi. Flying laser range sensor for large-scale site-modeling and its applications in bayon digital archival project. *IJCV*, 2008.

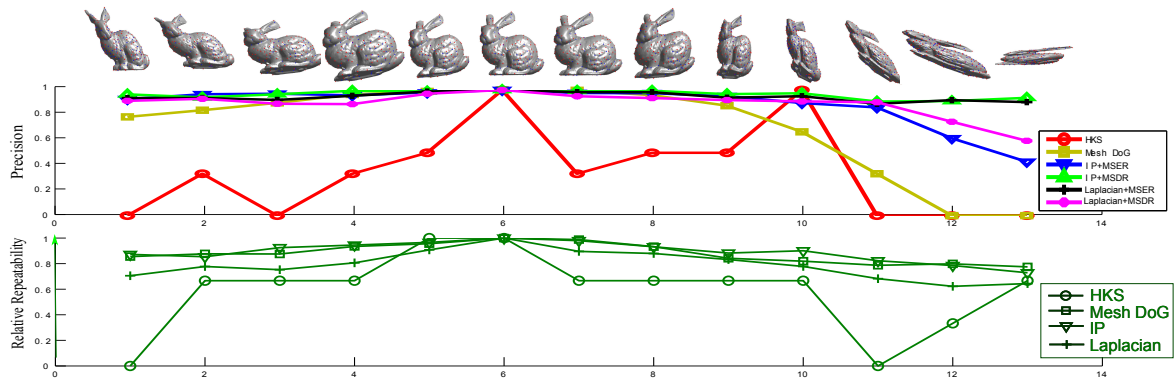


Figure 7. Matching precision and Relative Repeatability in comparison with HKS [22] and Mesh DoG [25].

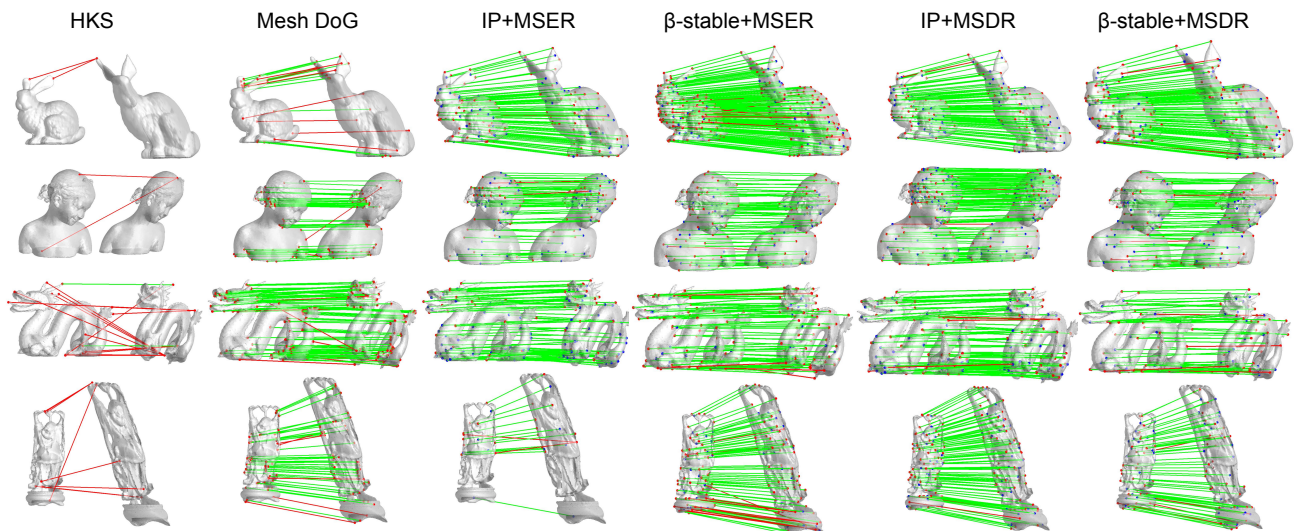


Figure 9. Matching results comparison from left to right: HKS [22], Mesh DoG [25], IP combined with MSER [16], Laplacian combined with MSER [16], IP combined with MSDR and Laplacian combined with MSDR.

- [4] O. M. Becker and M. Karplus. The topology of multidimensional potential energy surfaces: Theory and application to peptide structure and kinetics. *J. Chem. Phys.*, 106, 1997.
- [5] M. Bronstein and I. Kokkinos. Scale-invariant heat kernel signatures for non-rigid shape recognition. In *CVPR*, 2010.
- [6] F. Cao, J. Lisani, J. Morel, P. Muse, and F. Sur. *A Theory of Shape Identification*. Springer Verlag, 2008.
- [7] J. Digne, J.-M. Morel, N. Audfray, and C. Mehdi-Souzani. The level set tree on meshes. In *Proc. 3DPVT*, 2010.
- [8] G. Flitton, T. Breckon, and N. Bouallagu. Object recognition using 3d sift in complex ct volumes. In *Proc. BMVC*, 2010.
- [9] M. Goresky and R. Macpherson. *Stratified Morse Theory*. Springer-Verlag, 1980.
- [10] S. Gu, Y. Zheng, and C. Tomasi. Critical nets and beta-stable features for image matching. In *ECCV*, 2010.
- [11] S. P. H. L. J. Sahner, B. Weber. Extraction of feature lines on surface meshes based on discrete morse theory. In *VisSYM*, volume 27, 2008.
- [12] A. Johnson. *Spin-Images: A Representation for 3-D Surface Matching*. PhD thesis, CMU, 1997.
- [13] J. Knopp, M. Prasad, G. Willems, R. Timofte, and L. Gool. Hough transform and 3d surf for robust three dimensional classification. In *ECCV*, pages 589–602, 2010.
- [14] R. Litman, A. M. Bronstein, and M. M. Bronstein. Diffusion-geometric maximally stable component detection in deformable shapes. In *CAG*, volume 35, 2011.
- [15] J. Markoff. Google cars drive themselves, in traffic. *The New York Times*.
- [16] J. Matas, O. Chum, M. Urban, and T. Pajdla. Robust wide baseline stereo from maximally stable extremal regions. In *BMVC*, 2002.
- [17] A. Mian, M. Bennamoun, and R. Owens. On the repeatability and quality of keypoints for local feature-based 3d object retrieval from cluttered scenes. *IJCV*, 89, 2010.
- [18] J. Novatnack and K. Nishino. Scale-dependent/invariant local 3d shape descriptors for fully automatic registration of multiple sets of range images. In *ECCV*, 2008.
- [19] M.-T. Pham, O. Woodford, F. Perbet, A. Maki, B. Stenger, and R. Cipolla. A new distance for scale-invariant 3d shape recognition and registration. In *ICCV*, 2011.

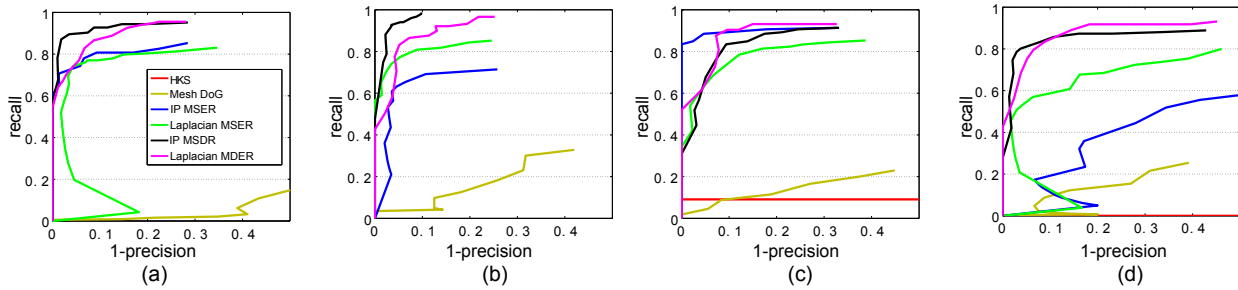


Figure 10. Comparison on recall v.s. (1-precision) graph. (a)-(d) are corresponding to 4 cases shown in Fig. 9.

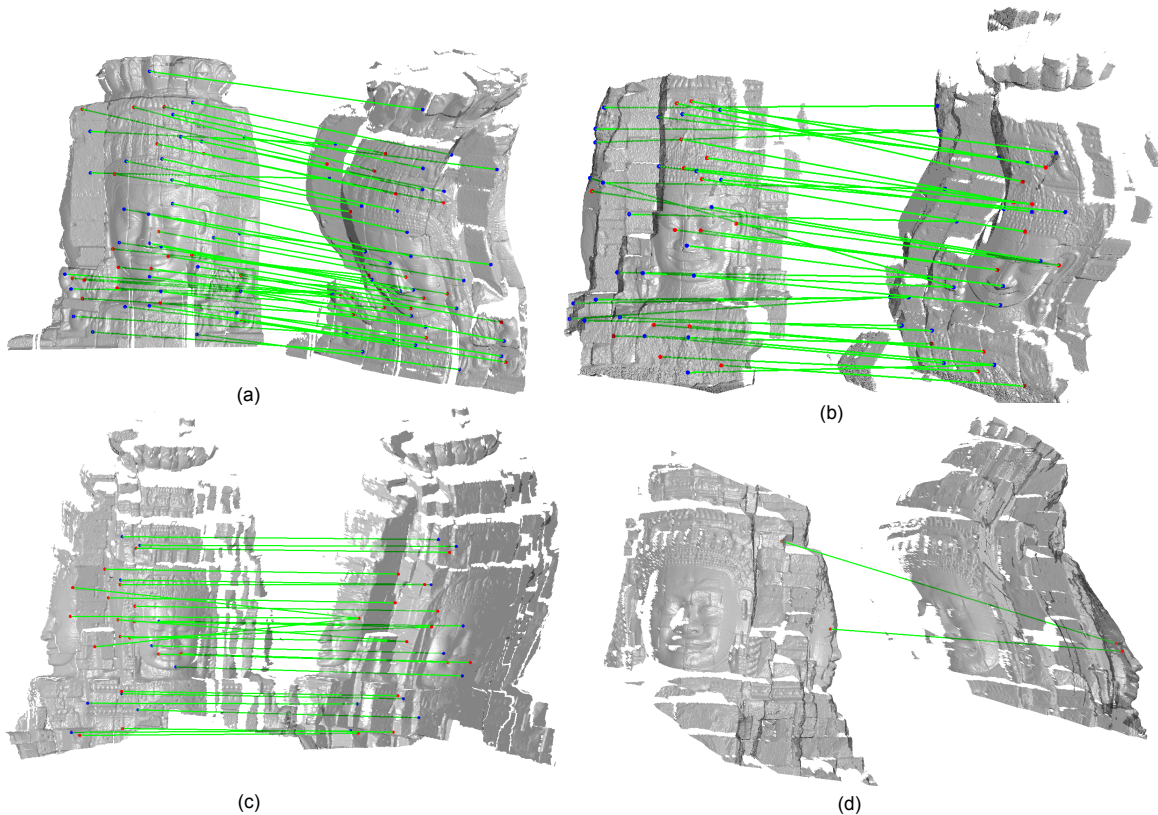


Figure 11. Real data matching results: acceptable results (a)-(c) and a failure case (d) due to the less overlaps.

- [20] Phoenix Aerial LiDAR. Velodyne presents successful implementation of hdl-32e lidar on uav at subexpo in san francisco. sUAS News.
- [21] D. Raviv, A. Bronstein, M. Bronstein, R. Kimmel, and N. Sochen. Affine-invariant diffusion geometry for the analysis of deformable 3d shapes. In *CVPR*, 2011.
- [22] J. Sun, M. Ovsjanikov, and L. Guibas. A concise and provably informative multi-scale signature based on heat diffusion. In *SGP*, 2009.
- [23] R. Unnikrishnan and M. Hebert. Multi-scale interest regions from unorganized point clouds. In *S3D*, 2008.
- [24] J. Wang and Z. Yu. Geometric decomposition of 3d surface meshes using morse theory and region growing. *Intl. Journal of Advanced Manufacturing Technology*, 56(9-12), 2011.
- [25] A. Zaharescu, E. Boyer, K. Varanasi, and R. Horaud. Surface feature detection and description with applications to mesh matching. In *CVPR*, pages 373–380, 2009.
- [26] B. Zheng, R. Ishikawa, J. Takamatsu, K. Ikeuchi, T. Endo, K. Sato, T. Ueno, T. Sugie, M. Toi, S. Kanao, and K. Togashi. Breast mr image fusion by deformable implicit polynomial (dip). *IPSJ CVA*, 5, 2013.
- [27] B. Zheng, Y. Sun, J. Takamatsu, and K. Ikeuchi. A feature descriptor by difference of polynomials. *IPSJ CVA*, 5, 2013.
- [28] B. Zheng, J. Takamatsu, and K. Ikeuchi. An adaptive and stable method for fitting implicit polynomial curves and surfaces. *TPAMI*, 32(3):561–568, march 2010.